Photocarrier-induced reduction of the lifetime of acoustic phonons in semiconductor superlattices

María Florencia Pascual-Winter,[1,2,*] Alejandro Fainstein,[1]
Bernard Jusserand,[2] Bernard Perrin,[2] and Aristide Lemaître[3]

[1] *Centro Atómico Bariloche & Instituto Balseiro, C.N.E.A., R8402AGP San Carlos de Bariloche, Argentina*
[2] *Institut des Nanosciences de Paris, CNRS, Université Paris 6, Campus Boucicaut, 140 Rue de Lourmel, 75015 Paris, France*
[3] *Laboratoire de Photonique et de Nanostructures, CNRS, Route de Nozay, 91460 Marcoussis, France*

(Received April 12, 2010)

We present an experimental analysis of the role of the electron–phonon interaction in the lifetime of coherent longitudinal acoustic phonons in a sample based on the GaAs/AlAs superlattice structure. Sub-terahertz phonons are generated and detected through an ultra-fast pump-probe technique. In order to supply with different scenarios for the electron–phonon interaction, two experimental configurations are proposed, either with a high or a nil density of photo-excited carriers in the spatial region where the phonon detection takes place. We observe a one-order-of-magnitude reduction in the phonon lifetime in the first case with respect to the second.

PACS numbers: 63.22.Np, 71.38.-k, 78.47.D-

I. INTRODUCTION

Coherent longitudinal acoustic phonons are envisaged for applications in electronics, optoelectronics, phonon spectroscopy, and nanoscopy. Interesting experiments leading the pathway towards each of the mentioned applications have been published recently. To highlight just a few, we may cite in the electronics domain the transport of charge induced by acoustic pulses reported by Fowler *et al.* [1]; in optoelectronics, the ultra-fast control of the quantum well emission by optically generated acoustic pulses presented by Scherbakov and co-workers [2]; in phonon spectroscopy, the determination of the specific heat in two-dimensional electronic systems through the absorption of an acoustic pulse demonstrated by Zeitler *et al.* [3]; and in nanoscopy, the access to the structure of interfaces in multilayered samples through the analysis of the shape of acoustic echo signals reported by Rossignol and colleagues [4]. In most of the listed experiments, the acoustic vibrations are coherently generated by a femtosecond optical pump pulse, and in some cases, the effect of those vibrations is also monitored by a second delayed optical probe pulse. Thus, a great deal of effort has been devoted to gather phenomenology of such processes as well as to understand the physics behind. Multilayered nanostructures such as superlattices (SLs) or quantum

wells have been most preferably chosen due to the possibility they offer for tailoring the acoustic, electronic and optical properties of the sample. The works of Mishina *et al.* [5] and Bartels *et al.* [6] have been particularly enlightening for identifying the acoustic modes involved in typical pump-probe experiments. Further knowledge towards identifying the individual effects of the generation and detection mechanisms has been provided by the work of Mizoguchi *et al.,* who reported a two-color experiment (different wavelengths for the pump and probe optical pulses) [7], and by Trigo *et al.* [8], Huynh *et al.* [9] and the authors of the present article [10], who spatially separated the generation and detection processes in different regions of the sample. The subject of the lifetime of a photo-generated acoustic population has been little quantitatively explored both in bulk samples [11–13] and in SLs [14, 15]. Very little is known also about the attenuation mechanisms. Inhomogeneous broadening and scattering by defects have been proposed as important mechanisms for phonon attenuation in superlattices [15] as well as anharmonic effects [14].

In the present study, we aim at exploring the importance of the electron-phonon interaction in the lifetime of acoustic phonons in the sub-terahertz range. As we mentioned above, phonons are generally generated by an optical pulse. For the generation to be efficient, it has been phenomenologically shown that the optical wavelength must be close to electronic interband transitions of the sample (see for example Ref. [14]). It is therefore expectable that under such a condition, a non-negligible population of electron–hole pairs will be created by the pump pulse. This high density of photo-excited carriers is thus an important source of scattering centers for phonons. This effect is studied in the experiments described below. In order to provide with different scenarios for the electron–phonon interaction, we propose two experimental configurations for the phonon generation and detection processes in a sample consisting of two GaAs/AlAs superlattices separated by a thick intermediate GaAs layer. In one of these configurations, the phonons are detected in a region of strong density of photo-excited carriers, while in the other, the phonons are detected in the absence of carriers.

The rest of the article is organized in five sections with self-explanatory titles. We shall begin by the sample description.

II. DESCRIPTION OF THE SAMPLE

The sample consisted of two 100-period GaAs/AlAs SLs grown by molecular beam epitaxy (MBE) on either side of a double-sided-polished 356-mm-thick [001]-oriented GaAs substrate (see Fig. 1(a)). Both SL periods were chosen so that the first minigap in the zone-center of the folded longitudinal acoustic branch of the phonon dispersion relation falls at a frequency of 0.4 THz. The thicknesses d_{GaAs} and d_{AlAs} of the GaAs and AlAs layers within one SL period fulfilled the conditions $d_{\mathrm{GaAs}} = 3v_{\mathrm{GaAs}}/(4\nu_0)$ and $d_{\mathrm{AlAs}} = v_{\mathrm{GaAs}}/(4\nu_0)$, respectively, which maximizes the width of the first zone-center minigap centered at a frequency ν_0 (v_{GaAs} and v_{AlAs} are the sound velocities of longitudinal acoustic phonons in each material). These relations yield nominal values $d_{\mathrm{GaAs}} = 88.6$ Å and $d_{\mathrm{AlAs}} = 35.2$ Å, which were entered for the MBE growth process. However, during the growth of one of

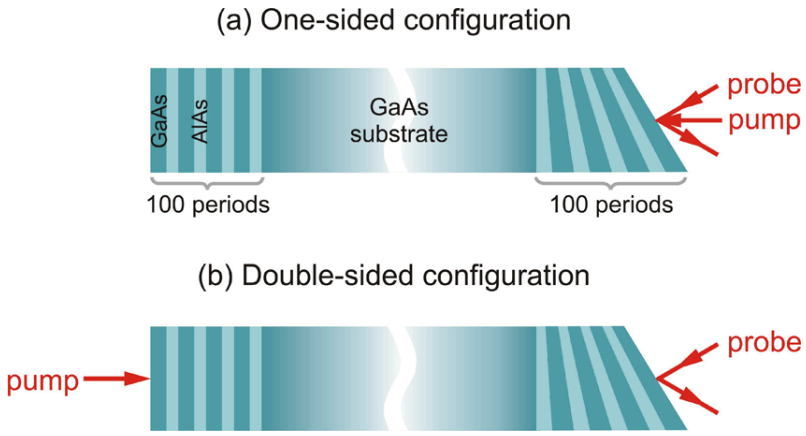

FIG. 1: cheme of the sample and experimental configurations. (a) One-sided configuration: the pump and probe beams shine on the same surface of the sample. (b) Two-sided configuration: the pump beam shines on the uniform SL, and the probe beam reflects off the tapered SL.

the SLs, the spinning of the substrate wafer was suppressed in order to obtain a tapered SL, i.e., a gradient in the thicknesses of all the layers. X-ray experiments returned the values $d_{\mathrm{GaAs}} = 89$ Å and $d_{\mathrm{AlAs}} = 35$ Å for the uniform (nontapered) SL and $d_{\mathrm{GaAs}} = 88$ Å and $d_{\mathrm{AlAs}} = 35$ Å in the center of the tapered one. Pump-probe experiments revealed a thickness gradient of $\sim 22\%$ along the direction of maximum gradient of the wafer, from one of its ends diametrically to the opposite. (The value of the gradient was inferred from the energy shift of the folded acoustic modes in the pump-probe spectra.)

The aim of the thickness gradient was to add a degree of freedom that would allow us to match the otherwise detuned spectral responses of the phonon generation and phonon detection processes, as reported in earlier works [10, 16]. The position on the wafer where spectral matching was achieved was carefully sought through pump-probe experiments performed as a function of position to be reported elsewhere (equivalent to those described in Ref. [10]).

III. EXPERIMENT

Interferometric pump-probe experiments [17] were performed at room temperature at a laser wavelength of 750 nm and at a temperature of 15 K. Femtosecond pulses (~ 80 fs) from a mode-locked Ti:sapphire laser, with a repetition rate of 81.8 MHz, were split into the pump and probe pulses. The pump was modulated at 1.8 MHz by an acousto-optic device in order to allow for synchronous detection through a lock-in amplifier. Both pulses were focused onto ~50-mm-diameter spots. For testing the effect of the electron–phonon interaction in the phonon lifetime, two configurations were used (depicted in Fig. 1): in the henceforth called *one-sided configuration,* both the pump and probe beams shone the same side of the sample (see Fig. 1(a)); in the henceforth called *double-sided configuration,*

the pump beam impinged upon the uniform SL, while the probe beam reflected off the tapered SL (see Fig. 1(b)). The one-sided configuration is the standard one in pump-probe experiments. The double-sided one needs a more exigent alignment protocol since beams arriving at opposite ends of the sample must be focused on the same (x,y) position ($\hat{\mathbf{z}}$ is the sample growth axis) [18]. For the double-sided configuration, the energies used for the pump and probe pulses were 3.4 nJ and 2.0 nJ, respectively. In the one-sided configuration, the pump energy was reduced to 0.8 nJ in order to avoid saturation of the lock-in amplifier due to intense electronic and thermal contributions to the detected signal (these contributions are absent in the double-sided configuration since they are only appreciable in the region covered by the penetration depth of the pump beam); the probe pulse energy was the same as in the double-sided configuration. Care was taken to assure that the experiments carried out in both configurations were performed on the same (x,y) position on the sample.

The spectral tuning of the generation and detection responses by means of the thickness gradient is of course only available when the experiment is performed in the double-sided configuration. In the one-sided configuration, some small overlap between the generation and detection spectral responses (and a consequent nonzero pump-probe signal) is assured by the presence of oscillations in both spectra which result from the finite size of the SL [19–21] (light absorption, if any, also contributes to an increase in the overlap of the spectral responses because of wave vector conservation relaxation). The signal is nevertheless expected to be smaller in the one-sided configuration than in the tuned double-sided one.

IV. RESULTS

The normalized pump-probe signals as a function of the time delay between the pump and the probe pulses are plotted for both configurations shown in Fig. 2(a) and 2(c). The vertical axis displays the signal obtained in the interferometric experimental scheme, noted as $\Delta\Phi$ [22]. The signals have been numerically band-pass filtered in order to extract the first zone-center acoustic modes out of other contributions to the signal such as the Brillouin mode (low-energy acoustic mode) and thermal and electronic contributions (these are only present in the one-sided configuration, though). The passing band of the filter comprised the region around the first zone-center minigap, and its width was chosen in order not to miss any of the expected modes. In the case of the one-sided configuration, an experimental artifact introduced an oscillation of frequency very close to the region of interest. Therefore, a very sharp profile of the passing band had to be used. This is the origin of the strong oscillation in Fig. 2(a) at times t shorter than 100 ps. Thus, the region $0 \leq t < 100$ ps should not be considered for further analysis. Large time values in the x-axis of Fig. 2(c) are the result of the transit time of the phonons through the 356-μm-thick substrate placed between the SLs. Indeed, the increasing shape of the signal at the position of the arrow shown in Fig. 2(c) denotes the arrival of the phonons at the detection SL (the tapered SL). Comparison of Fig. 2(a) and 2(c) reveals a marked difference in the decay time of the signal depending on the configuration. The one-sided configuration exhibits a much faster decay

time, approximately one order of magnitude faster. We also observe beatings in both time traces. The beating rhythm in the one-sided configuration is also much faster than that in the double-sided one, revealing frequency components farther away from the signal.

The Fourier analysis of the time traces is presented in Fig. 2(b) and 2(d). The quantity assigned to the y-axis of the graph is the Fourier transform modulus of the *time derivative* of the signal (which is equivalent to multiplying the Fourier transform of the signal by the frequency). The derivative is taken so that the electronic and thermal low frequency tail that usually hinders the acoustic peaks is eliminated. In the case of the one-sided configuration, the Fourier spectrum presents two main peaks at 0.39 and 0.43 THz. The first can be traced down to a detection peak, i.e., an energy at which the detection process is most sensitive, while the second peak is assigned to the generated mode, that is, the energy at which the generation process is most efficient (the phonon-induced variations in sample reflectivity coefficient, which are at the origin of the pump-probe signal, show a spectrum proportional to the product of the generation and detection spectra [23]). The assignment of the observed peaks to either the generation or detection process is supported by calculations not shown in the present article. The frequency separation between the peaks explains the beating in the time trace. With regard to the width of the modes, the generation and detection peaks present full widths at half maximum (FWHM) of 8 GHz and 5 GHz, respectively. In principle, neglecting any anharmonic interaction or dephasing mechanism, the decay time and FWHM of the modes is determined by the time interval the vibrations "spend" in the detection region of the sample before escaping to the substrate (folded acoustic modes are no longer able to be detected by a probe pulse when they propagate along the substrate). In the one-sided configuration, this region coincides with the region where the phonons are generated by the pump pulse, and this is no other than the SL upon which both pulses impinge. Thus, the decay time of the modes should match the transit time of each mode through the SL. To estimate such transit time, we must consider the sound velocity of the modes. In the case of the detection one, as it is situated off zone-center (its wave vector differs from zone-center in twice the photon wave vector), it falls in a straight region of the dispersion relation. Its sound velocity is thus the slope of this straight line. Estimations of this slope [24] and the total length of the SL yield an expected value of 2.2 GHz, which is below the experimental result. In the case of the generation mode, the discrepancy between theory and experiment is even more striking since the sound velocity is much slow due to the bending of the dispersion relation very close to zone-center [24]. Calculations yield an expected FWHM of 0.4 GHz, 20 times less than the experimental value.

With regard to the double-sided configuration, the Fourier analysis shown in Fig. 2(d) exhibits one main peak situated at an energy that coincides with the detection peak of Fig. 2(b). As the detection in both the one- and double-sided configurations takes place in the same SL (see Fig. 1), this spectral "coincidence" assures that the (x,y) position on the sample where the experiment was performed had been properly chosen as far as the spectral overlap of the generation and detection efficiencies is concerned. The observation of just one peak shows that the energies of the generation and detection peaks actually match. A closer look at the experimental peak (see the inset of Fig. 2(d)) reveals some structure and side oscillations. Both features can be traced down to SLs-finite-size effects,

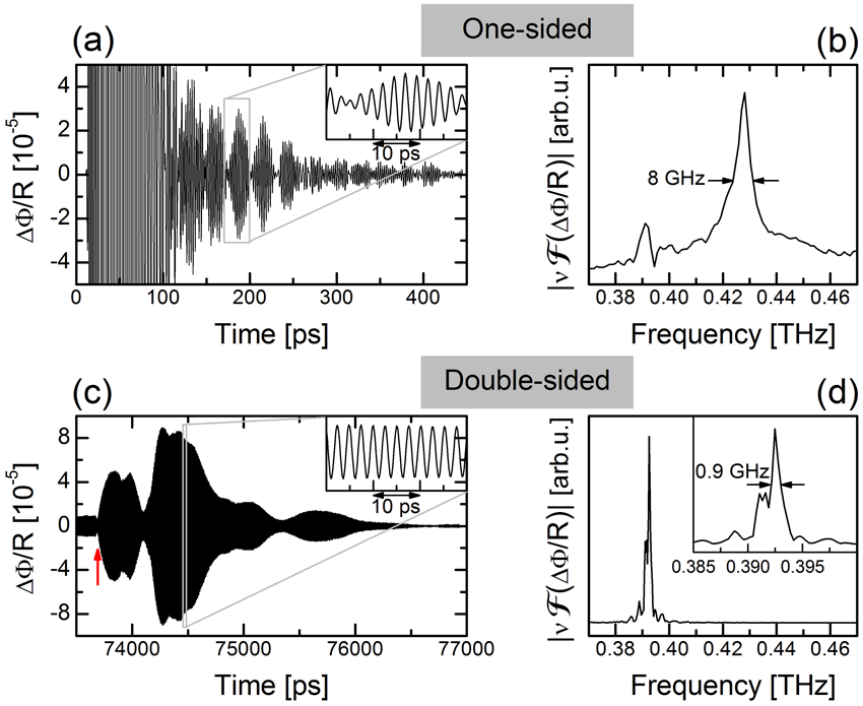

FIG. 2: Experimental results obtained in the one-sided configuration ((a) and (b)) and in the double-sided configuration ((c) and (d)). (a) and (c): Normalized interferometric pump-probe signal [22] as a function of the time delay between pump and probe pulses. The traces have been numerically filtered in order to eliminate the electronic, thermal and Brillouin contributions to the signal. In (c), the arrow indicates the instant at which phonons arrive at the tapered SL from the substrate. (b) and (d): Fourier transform of the time derivative of the normalized interferometric pump-probe signal ($\Phi(f)$ denotes the Fourier transform operation on f), which is equivalent to the product of the frequency and the Fourier transform of the normalized signal.

and they are responsible for the beating in the time trace. The FWHM of the main peak is 0.9 GHz, almost an order of magnitude smaller than the FWHM of the generation peak in the one-sided configuration. Nevertheless, this value is more than twice the expected value of 0.4 GHz [25].

We shall address possible reasons for the highlighted discrepancies between both the configurations and between the experiment and the theory in the following section.

V. DISCUSSION

Possible reasons for mode broadening are interactions with other excitations in the material (homogeneous broadening) and fluctuations in the structural characteristics of the sample within the region under study, typically thickness fluctuations in the layers (inhomogeneous broadening). The latter are not able to explain our experimental observations

because the same SL that returns broad peaks in the one-sided configuration is also involved in the double-sided configuration. If we momentarily assume that, for some reason, thickness fluctuations have a much more important effect on the generation process than on the detection one, we could argue that the discrepancy between the peaks' FWHM in one configuration and in the other configuration might be explained through a marked difference of growth quality between the SLs. This is not the case as we have verified the quality of both SLs by means of X-ray diffraction, resonant Raman scattering and photoluminescence excitation experiments. Although a slightly lower quality in the tapered SL was observed, the difference was far too small to explain the experimental results. If we thus turn to homogeneous broadening, neither can anharmonic terms in the Hamiltonian of the phonon system (decomposition of the phonon in lower energy modes satisfying energy and wave vector conservation) justify the discrepancy since the frequency range of the phonons in both configurations is very similar. An irrefutable argument is also that the double-sided configuration phonons need to outlive a ∼74-nanosecond transit time through the intermediate substrate to arrive from one SL to the other. If some anharmonic effect took place, the maximum broadening compatible with the mentioned transit time would be absolutely negligible with respect to the experimental FWHM. One last argument concerning anharmonic phonon decay can be sought in the temperature difference of the SL in which the detection takes place in each configuration. The temperature of the detection SL is higher in the one-sided configuration since the heating caused by the pump pulse occurs in the same SL where phonons are detected. In the double-sided configuration, this heating takes place at the opposite end of the sample. We could think of this as an asymmetry between the configurations that might in some way result in a phonon lifetime difference. However, it is worth noting that the temperature difference can be estimated to only some tenths of kelvin, for which this argument must also be discarded.

As the phonon–phonon interaction has been ruled out, we turn now to the electron–phonon interaction. In fact, there is a non-negligible asymmetry between configurations with regard to the density of photo-excited carriers in the region of the detection SL. In the one-sided configuration, pump and probe pulses impinge upon the same SL. Therefore, the phonons that are detected by the probe pulse live in a region of high density of carriers photo-excited by the pump pulse. On the contrary, in the case of the double-sided configuration, the phonons that are detected are, in fact, those that have been able to escape the region of high photo-excited carriers toward the substrate. Once they leave the penetration depth of the pump beam (of the order of 1 μm), their lifetime is no longer limited by the electron–phonon interaction. This is therefore our hypothesis for explaining a broad line in the generation mode in the one-sided configuration and a narrow one in the double-sided configuration. Additional experimental data show that the 750-nm laser is close to an electronic resonance condition, which allows us to expect a high population of photo-excited carriers. Complementary experimental verification of the hypothesis should be sought in pump-power dependent experiments.

It is noteworthy that the explanation just given should, in principle, predict the same linewidth for both the generation and detection modes in the one-sided configuration unless zone-center (generation) modes and off-zone-center (detection) modes interact differently

with carriers (we recall that the experimental information is that the detection mode is narrower that the generation one: 5 GHz vs. 8 GHz). In fact, continuum model calculations of the elastic energy spatial distribution of the acoustic modes predict a particular concentration of elastic energy in the SL region in the case of the generation mode (see Fig. 1 of Ref. [26]). The elastic energy in the detection mode is somewhat more uniformly distributed between the substrate and the SL [26]. It is therefore expected that the generation mode's lifetime will be more strongly affected by the electron-phonon interaction.

Finally, we address the fact that the experimental FWHM of the peak in the double-sided configuration (0.9 GHz) is larger than the theoretical value of 0.4 GHz. We attribute this discrepancy to the broadening introduced by structural imperfections of the sample: thickness fluctuations and/or the scattering of phonons by defects. Although these effects are unable to explain a configuration-dependent linewidth, this does not mean that they are not at all present in our experiments. The experimental data just allow us to state that they are less important than the electron–phonon interaction effect in the case in which the latter takes a relevant role (the one-sided configuration). In the double-sided configuration, in which photocarriers are absent in the detection region, the broadening effects left are inhomogeneous broadening and/or scattering at defects. They are both also compatible with the fact that the phonons outlive the travel time through the substrate, for these broadening mechanisms start off only when the phonons enter the detection SL.

VI. CONCLUSIONS

We have presented experimental results that reveal the importance of the electron–phonon interaction in the lifetime of sub-terahertz longitudinal acoustic phonons. In order to test the effect of scattering of phonons by carriers photo-excited by the pump pulse, we have made use of two experimental configurations differing in the presence or absence of photocarriers in the spatial region of phonon detection. In the first case (pump and probe beams impinging upon the same SL), a one-order-of-magnitude reduction in the phonon lifetime was found with respect to the second scenario (pump and probe beams impinging upon the opposite ends of the sample). The possibility of other line-broadening effects has also been analyzed. Although discarded for justifying the configuration-dependent lifetime of the acoustic mode, inhomogeneous broadening and/or scattering of phonons by defects are needed to explain experiment/theory discrepancy in the mode line width in the absence of photocarriers. Nevertheless, when the latter are present in a high density, the limiting factor to the phonon lifetime is the electron–phonon interaction.

References

* Electronic address: pascualm@ib.cnea.gov.ar

[1] D. R. Fowler, A. V. Akimov, A. G. Balanov, M. T. Greenaway, M. Henini, T. M. Fromhold, and A. J. Kent, Appl. Phys. Lett. **92**, 232104 (2008).

[2] A. V. Scherbakov, T. Berstermann, A. V. Akimov, D. R. Yakovlev, G. Beaudoin, D. Bajoni, I. Sagnes, J. Bloch, and M. Bayer, Phys. Rev. B **78**, 241302(R) (2008).
[3] U. Zeitler, A. M. Devitt, J-E-Digby, C-J-Mellor, A. J. Kent, K. A. Benedict, and T. Cheng, Phys. Rev. Lett. **82**, 5333 (1999).
[4] C. Rossignol, J. M. Rampnoux, M. Perton, B. Audoin, and S. Dilhaire, Phys. Rev. Lett. **94**, 166106 (2005).
[5] T. Mishina, Y. Iwazaki, Y. Masumoto, and M. Nakayama, Solid State Commun. **107**, 281 (1998).
[6] A. Bartels, T. Dekorsy, H. Kurz, and K. Köhler, Phys. Rev. Lett. **82**, 1044 (1999).
[7] K. Mizoguchi, M. Hase, S. Nakashima, and M. Nakayama, Phys. Rev. B **60**, 8262 (1999).
[8] M. Trigo, T. A. Eckhause, J. K. Wahlstrand, R. Merlin, M. Reason, and R. S. Goldman, App. Phys. Lett. **91**, 23115 (2007).
[9] A. Huynh, B. Perrin, N. D. Lanzillotti-Kimura, B. Jusserand, A. Fainstein, and A. Lematre, Phys. Rev. B **78**, 233302 (2008).
[10] M. F. Pascual Winter, A. Fainstein, B. Jusserand, B. Perrin, and A. Lemaître, Appl. Phys. Lett. **94**, 103103 (2009).
[11] Chen, Maris, Wasilewski and Tamura, Philosophical Magazine B **70**, 687 (1994).
[12] T. C. Zhu, H. J. Maris, and J. Tauc, Phys. Rev. B **44**, 4281 (1991).
[13] J.-Y. Duquesne and B. Perrin. Phys. Rev. B **68**, 134205 (2003).
[14] M. F. Pascual Winter, G. Rozas, A. Fainstein, B. Jusserand, B. Perrin, A. Huynh, P. O. Vaccaro, and S. Saravanan, Phys. Rev. Lett. **98**, 265501 (2007).
[15] G. Rozas, M. F. Pascual Winter, B. Jusserand, A. Fainstein, B. Perrin, E. Semenova, and A. Lemaître, Phys. Rev. Lett. **102**, 015502 (2009).
[16] M. F. Pascual Winter, A. Fainstein, B. Jusserand, B. Perrin, and A. Lemaître, J. Phys.: Conf. Series **92**, 012013 (2007).
[17] B. Perrin, B. Bonello, J.-C. Jeannet, and E. Romatet, Prog. Natural Sci. **S6**, 444 (1996).
[18] J.-Y. Duquesne, and B. Perrin, Phys. Rev. B **68**, 134205 (2003).
[19] M. Nakayama, K. Kubota, H. Kato, and N. Sano, J. Appl. Phys. **60**, 3289 (1986).
[20] M. W. C. Dharma-wardana, Phys. Rev. B **48**, 11960 (1993).
[21] M. Trigo, A. Fainstein, B. Jusserand, and V. Thierry-Mieg, Phys. Rev. B **66**, 125311 (2002).
[22] $\Delta\Phi$ is related to the reflectivity coefficient r_0 of the sample in the absence of oscillations and to the contribution $\Delta r(t)$ introduced by the latter through the relation $\Delta\Phi(t) = -\mathbf{Re}(r_0)\mathbf{Im}(\Delta r(t)) + \mathbf{Im}(r_0)\mathbf{Re}(\Delta r(t))$ [17].
[23] N. D. Lanzillotti Kimura, A. Fainstein, A. Huynh, B. Perrin, B. Jusserand, A. Miard, and A. Lematre, Phys. Rev. Lett. **99**, 217405 (2007).
[24] B. Jusserand and M. Cardona, in *Raman Spectroscopy of Vibrations in Superlattices* (Topics in Applied Physics, Vol. 5: Light Scattering in Solids V), eds. M. Cardona and G. Güntherodt (Springer-Verlag, Berlin, Heidelberg, 1989).
[25] We compare the width of the experimental peak in the double-sided configuration to that of the theoretical *generation* peak because the experimental peak is the result of the product between a narrow peak (the generation peak) and a much wider one (the detection one). The resulting peak has mainly the width of the narrower mode.
[26] M. Trigo, T. A. Eckhause, M. Reason, R. S. Goldman, and R. Merlin, Phys. Rev. Lett. **97**, 124301 (2006).